CEAS EuroGNC 2022
"Conference on Guidance, Navigation and Control"
3-5 May 2022 @ Technische Universität Berlin, Germany

Optimal Variable Wing Camber Control using Incremental Nonlinear Dynamic Inversion

T. S. C. Pollack Ph.D. Student, Control and Simulation Division, Faculty of Aerospace Engineering, Delft University of Technology, 2629HS, Delft, The Netherlands. T.S.C.Pollack@tudelft.nl

E. van Kampen Assistant Professor, Control and Simulation Division, Faculty of Aerospace Engineering, Delft University of Technology, 2629HS, Delft, The Netherlands. E.vanKampen@tudelft.nl

ABSTRACT

Flight control systems enable the improvement of natural flying qualities and airframe performance of an aircraft. In this article, an incremental optimization control scheme is proposed to optimize a given performance objective set by the designer in an online fashion using limited model information. This scheme is applied to improve the aerodynamic efficiency levels of the General Dynamics F-16 by optimizing symmetric movement of the leading edge flap (LEF) devices, based on an open-source nonlinear simulation model. Other design goals are addressed by refining the control objective, which explicitly embeds design trade-offs in the control law. A complete control architecture is arrived at through the design of a parallel INDI control law that performs the function of angular rate control to improve natural flying qualities. A nonlinear simulation scenario shows that the proposed control framework is capable of meeting desired handling quality characteristics while simultaneously improving aerodynamic efficiency levels and control activity. In addition, a robustness assessment is performed to gain insight into the sensitivity of the design to on-board model offsets.

Keywords: Nonlinear Control, Incremental Control, Control Configuration Optimization

1 Introduction

Flight control systems typically need to fulfill several functionalities at both the pilot and airframe level, depending on the class of vehicle and intended operational mission(s). This is reflected by the sheer amount of design objectives and requirements that typically drive the flight control law development process. Ensuring satisfactory handling qualities throughout the flight envelope represents a significant category in this regard. This is reflected by the requirement guidelines listed in MIL-STD-1797 [1]. Similarly, a wide range of control system safety requirements shall be met, including those related to stability and robustness [2]. Other types of design objectives may focus on overall airframe performance aspects such as those related to aerodynamic and structural efficiency levels, which may originate from high-level vehicle design considerations.

The relevance of the airframe-centric performance aspect is illustrated by flight control system design concepts seen on recent production aircraft. In the civil transport domain, the Boeing 787 family features a trailing edge variable camber (TEVC) concept to reduce drag levels in cruise condition [3]. Likewise, the Airbus A350XWB family is equipped with an adaptive dropped hinge flap that enables

in-flight variable wing camber control to increase wing efficiency levels in off-design cruise conditions [4]. Similarly, modern fighter aircraft such as the Lockheed Martin F-22 and F-35 rely on an integrated composition of control surface movements to fulfil various functions, including adjustment of the airframe's aerodynamic profile [5, 6]. This has even enabled the removal of dedicated speedbrakes [7]. There is real interest in design philosophies that move towards multi-functional effector suites, which boils down to further integration of the flight control system architecture to meet design objectives [4].

There has been widespread interest in recent years in nonlinear robust control techniques that can alleviate or even circumvent the challenges posed by identification and modelling of possibly complex aerodynamics in the control law development process. One such category of control methods that has seen successful applications both in simulation and during flight tests is known as Incremental Non-linear Dynamic Inversion (INDI) [8–16]. INDI is based on the principles of feedback linearization and forms an incremental variant to Nonlinear Dynamic Inversion (NDI). It reduces the need for accurate on-board model (OBM) representations of the airframe aerodynamics by using sensor information instead. Existing studies have focused primarily on developing INDI-based manual control laws for improving natural flying qualities and autopilots for both aircraft and rotorcraft. In addition, INDI has been investigated for use in gust and maneuver load alleviation control systems [17–19]. Another line of research focuses on incremental control allocation schemes, which have been considered for optimization of secondary control objectives such as the $\mathscr{L}_2$-norm of weighted control deflections [20] or other airframe configuration and performance targets [21–23]. Such allocation schemes can be regarded as examples of multi-functional flight control design. However, to the authors' best knowledge, using the principles of INDI to directly optimize effector configurations based on aerodynamic performance objectives has not been widely addressed, despite the fact that these objectives may be driving factors in the design process.

The contribution of this article is twofold. First, an incremental optimal control scheme that enables online optimization of a given design objective using dedicated control effectors is proposed, which is introduced in Section 2. Second, this scheme is used to develop an incremental optimal control[1] law in the context of variable wing camber control to improve the aerodynamic efficiency levels of an open-source General Dynamics F-16 nonlinear aircraft model, which is described in Section 3. The proposed control system is applied in a nonlinear simulation study, the results of which are presented in Section 4. Section 5 concludes the article and provides recommendations for further research.

2 Fundamental Principles

In this Section, the fundamental properties of the incremental control techniques considered in this study are described. First, the basic derivations associated with the Incremental Nonlinear Dynamic Inversion (INDI) design framework are reviewed in Subsection 2.1. This is followed by a formulation of the proposed INDI-based optimal control strategy, which is introduced in Subsection 2.2.

2.1 Incremental Nonlinear Dynamic Inversion (INDI)

Consider a nonlinear multi-input multi-output (MIMO) square system Σ of the form

$$\Sigma : \begin{cases} \dot{x} = f(x) + g(x,u) \\ y = h(x) \end{cases} \tag{1}$$

described by the state vector $x \in \mathbb{R}^n$, the input vector $u \in \mathbb{R}^m$, the observation vector $y \in \mathbb{R}^m$, and smooth mappings f, g, and h. If it holds that $g(x,u) = G(x)u$, which implies that the system is input-

---

[1]The terminology chosen here does not refer to classical optimal control theory, which aims at synthesizing controllers that optimize dynamic system trajectories; instead, this work focuses on minimization of a system output that serves as a control objective selected by the designer.

affine, a traditional Nonlinear Dynamic Inversion (NDI) control law can be derived by taking repeated Lie derivatives of the system output until the input vector u appears in the output dynamics [24]. Without loss of generality, assuming for simplicity that the relative degree ρ of the system is equal to one for all channels - which holds typically for aircraft rotational dynamics - the output dynamics are found as

$$\dot{y} = \frac{\partial h}{\partial x}\left(f(x) + G(x)u\right) = \begin{bmatrix} \mathscr{L}_f h_1(x) \\ \vdots \\ \mathscr{L}_f h_m(x) \end{bmatrix} + \begin{bmatrix} \mathscr{L}_{g_1} h_1(x) & \cdots & \mathscr{L}_{g_m} h_1(x) \\ \vdots & \ddots & \vdots \\ \mathscr{L}_{g_1} h_m(x) & \cdots & \mathscr{L}_{g_m} h_m(x) \end{bmatrix} u \triangleq \alpha(x) + \mathscr{B}(x)u \quad (2)$$

where $\mathscr{L}_f h_i(x)$ and $\mathscr{L}_{g_i} h_i(x)$ are defined as the Lie derivatives of the function h_i along the vectors fields described by f and g_i, with g_i being a column vector of the matrix G [24]. Assuming that the on-board model (OBM) representation of the control effectiveness matrix $\hat{\mathscr{B}}^{-1}(x)$ is invertible, this expression forms the basis for constructing the NDI control law,

$$u = \hat{\mathscr{B}}^{-1}(x)\left[v - \hat{\alpha}(x)\right] \quad (3)$$

The pseudo-control input vector v is generated by an auxiliary control loop and further determines the nominal and robust response characteristics associated with regulation or tracking by the control system. In the absence of uncertainty and additional high-order dynamics, closing the loop renders the output response to a set of m decoupled integrators, as reflected by

$$\dot{y} = v \quad (4)$$

To design the NDI control law in incremental form instead, the assumption that Σ is affine in the input can be dropped, which leads to a more general formulation of the output dynamics,

$$\dot{y} = \frac{\partial h}{\partial x}\left(f(x) + g(x,u)\right) \triangleq \alpha(x) + \beta(x,u) \quad (5)$$

An explicit feedback law for the control input u can be derived by performing a Taylor expansion of the output dynamics at time $t - \Delta t$ [25, 26], where Δt represents the sampling interval. Denoting this as time $t = 0$ for simplicity of notation, this results in the expression

$$\dot{y} = \dot{y}_0 + \left.\frac{\partial\left[\alpha(x) + \beta(x,u)\right]}{\partial x}\right|_0 \underbrace{(x - x_0)}_{\Delta x} + \left.\frac{\partial \beta(x,u)}{\partial u}\right|_0 \underbrace{(u - u_0)}_{\Delta u} + R_1 \quad (6)$$

Further simplification of this result is required to arrive at the final INDI control law, which is possible if the assumption of time-scale separation holds. This implies that the terms associated with the incremental state Δx and the expansion residual R_1 can be neglected, which is often the case in practice if sufficiently high sampling rates and fast actuation systems are available [8, 11, 26]. Subsequently, defining $\mathscr{B}(x,u) \triangleq \frac{\partial}{\partial u}\beta(x,u)$ and assuming that this term is invertible, the incremental equivalent of the NDI control law is found as

$$u = u_0 + \hat{\mathscr{B}}^{-1}(x_0, u_0)\left[v - \dot{y}_0\right] \quad (7)$$

Comparing equations 3 and 7 reveals that the INDI law requires less model information in case sensor measurements of the previous input vector and derivative of the control variable are available.

2.2 Incremental Optimal Control

In addition to performance requirements associated with disturbance rejection or reference tracking, the system Σ may need to satisfy other types of design objectives that call for optimal regulation of a range of output variables of interest. Such a design goal can be captured by formulating a scalar objective function $J \in \mathbb{R}$, which shall be minimized by an admissible control vector $u \in \mathscr{U} \subset \mathbb{R}^m$:

$$\min_{u \in \mathscr{U}} J(x, u) \tag{8}$$

Optimal control candidates can be found by considering the critical points associated with J, which may be within or outside the domain $\mathscr{U} \subset \mathbb{R}^m$. Consequently, the control target will be formulated as

$$J_u(x, u) = \frac{\partial J(x, u)}{\partial u}^T \to 0 \tag{9}$$

Effectively, a control law needs to be found that renders $J_u(x, u)$ to zero as closely as possible. Considering the fact that the function described by Equation 9 is in general non-affine in the input, the incremental design philosophy of taking the Taylor expansion can be invoked, which leads to

$$J_u(x, u) = J_u(x_0, u_0) + \left. \frac{\partial J_u(x, u)}{\partial x} \right|_0 \Delta x + \left. \frac{\partial J_u(x, u)}{\partial u} \right|_0 \Delta u + R_1 \tag{10}$$

Leveraging the time-scale separation assumption as before, a unique control solution exists that can be obtained directly by inversion if the control Hessian $H_u(x, u) \triangleq \frac{\partial}{\partial u} J_u(x, u)$ is non-singular:

$$u = u_0 - \hat{H}_u^{-1}(x_0, u_0) \hat{J}_u(x_0, u_0) \tag{11}$$

Since the control target described by Equation 9 does not make any distinction between local maxima or minima, an additional measure needs to be taken to arrive at the final optimal control law. Since the nature of the critical point can be deduced from the nature of $H_u(x, u)$, this information can be used to introduce control trajectories that are attracted to or repelled from the control target. In case the control input is scalar ($m = 1$), the sign of the second derivative can be used to this end. Consequently, taking the absolute value of the second-order derivative of J results in the desired behavior:

$$u = u_0 - \left[\left| \widehat{\frac{\partial^2 J(x, u)}{\partial u^2}} \right| \right]_0^{-1} \left[\widehat{\frac{\partial J(x, u)}{\partial u}} \right]_0 \tag{12}$$

As a result, a performance-optimizing control law is obtained that brings similar model mitigation benefits as the traditional INDI feedback law described by Equation 7. It is fully deterministic by nature, which gives it a natural advantage over adaptive or learning alternatives. However, the optimization problem in the presented form is unconstrained, which implies that e.g. control surface limits are not taken into account. Finally, it should be noted that the control law is reminiscent of the well-known Newton-Raphson numerical optimization method [27].

3 INDI-based Control Design for Optimized Airframe Performance

In this Section, incremental inversion-based control laws are developed for an open-source General Dynamics F-16 aircraft model [28, 29] that augment the bare airframe dynamics in terms of stability, handling qualities, and aerodynamic performance. The design goals and requirements are discussed in more detail in Subsection 3.1, which is followed by a brief description of the aerodynamic database in Subsection 3.2. Finally, the control law design process is presented in Subsection 3.3.

3.1 Design goals and requirements

Three main categories of design objectives and requirements are of interest in this study, including satisfactory handling qualities (*HQ*), maximal aerodynamic performance (*AP*), and minimal control effort (*CE*). An overview of high-level design criteria is included in Table 1. Note that a proper design assessment would also address minimum stability margin requirements, as specified in MIL-DTL-9490E [2]. However, this will be left for future design studies.

The nature of the aircraft system implies that the selected design criteria are interdependent to a large extent. This also depends on the available control architecture. The available aerodynamic control effectors include symmetric horizontal tail (HT), flaperons, rudder, and leading edge flap (LEF), which enables isolation of functionality across different channels to a large degree. This isolation of functionality is in accordance with the existing F-16 control system design philosophy, which relies on scheduling of the leading edge flap with angle of attack and dynamic pressure to e.g. maximize C_L/C_D [30].

Table 1   Overview of high-level control system design criteria

ID	Description	Source
HQ.1	Small-amplitude Low-Order Equivalent System (LOES) parameters should be well within Level-1 limits.	MIL-STD-1797A [1]
HQ.2	The control system should be free from objectionable transients throughout the service flight envelope.	MIL-STD-1797A [1]
AP.1	The aerodynamic efficiency level C_L/C_D should be maximized throughout the operational flight envelope.	-
CE.1	Control surface positions and rates should be limited for small-to-moderate stick activity.	-

3.2 Airframe Aerodynamics

The aerodynamic database of the nonlinear simulation model has been derived from low-speed static and dynamic (forced oscillation) wind-tunnel sub-scale test data and is described in [28]. The LEF database covers an angle-of-attack range of $-20° \leq \alpha \leq +60°$ and angle-of-sideslip range of $|\beta| \leq 30°$, respectively. The longitudinal force and moment coefficient equations are recited below; more detailed information, including a description of the lateral-directional aerodynamics, can be found in [28].

$$C_{X,t} = C_X(\alpha,\beta,\delta_h) + \Delta C_{X_{LEF}}\left(1 - \frac{\delta_{LEF}}{\delta_{LEF,max}}\right) + \frac{\bar{c}q}{2V}\left[C_{X_q}(\alpha) + \Delta C_{X_{q_{LEF}}}(\alpha)\left(1 - \frac{\delta_{LEF}}{\delta_{LEF,max}}\right)\right] \quad (13)$$

$$C_{Z,t} = C_Z(\alpha,\beta,\delta_h) + \Delta C_{Z_{LEF}}\left(1 - \frac{\delta_{LEF}}{\delta_{LEF,max}}\right) + \frac{\bar{c}q}{2V}\left[C_{Z_q}(\alpha) + \Delta C_{Z_{q_{LEF}}}(\alpha)\left(1 - \frac{\delta_{LEF}}{\delta_{LEF,max}}\right)\right] \quad (14)$$

$$C_{m,t} = C_m(\alpha,\beta,\delta_h)\eta_{\delta_h}(\delta_h) + C_{Z,t}(x_{CG,ref} - x_{CG}) + \Delta C_{m_{LEF}}\left(1 - \frac{\delta_{LEF}}{\delta_{LEF,max}}\right)$$
$$+ \frac{\bar{c}q}{2V}\left[C_{m_q}(\alpha) + \Delta C_{m_{q,LEF}}(\alpha)\left(1 - \frac{\delta_{LEF}}{\delta_{LEF,max}}\right)\right] + \Delta C_m(\alpha) \quad (15)$$

where

$$\Delta C_{(.)LEF} \triangleq \Delta C_{(.)LEF}(\alpha,\beta) - \Delta C_{(.)}(\alpha,\beta,\delta_h = 0°) \quad (16)$$

and δ_h and δ_{LEF} represent the horizontal tail and leading edge flap (LEF) control surface positions, respectively, x_{CG} represents the longitudinal center of gravity (CG) position in terms of %MAC, and
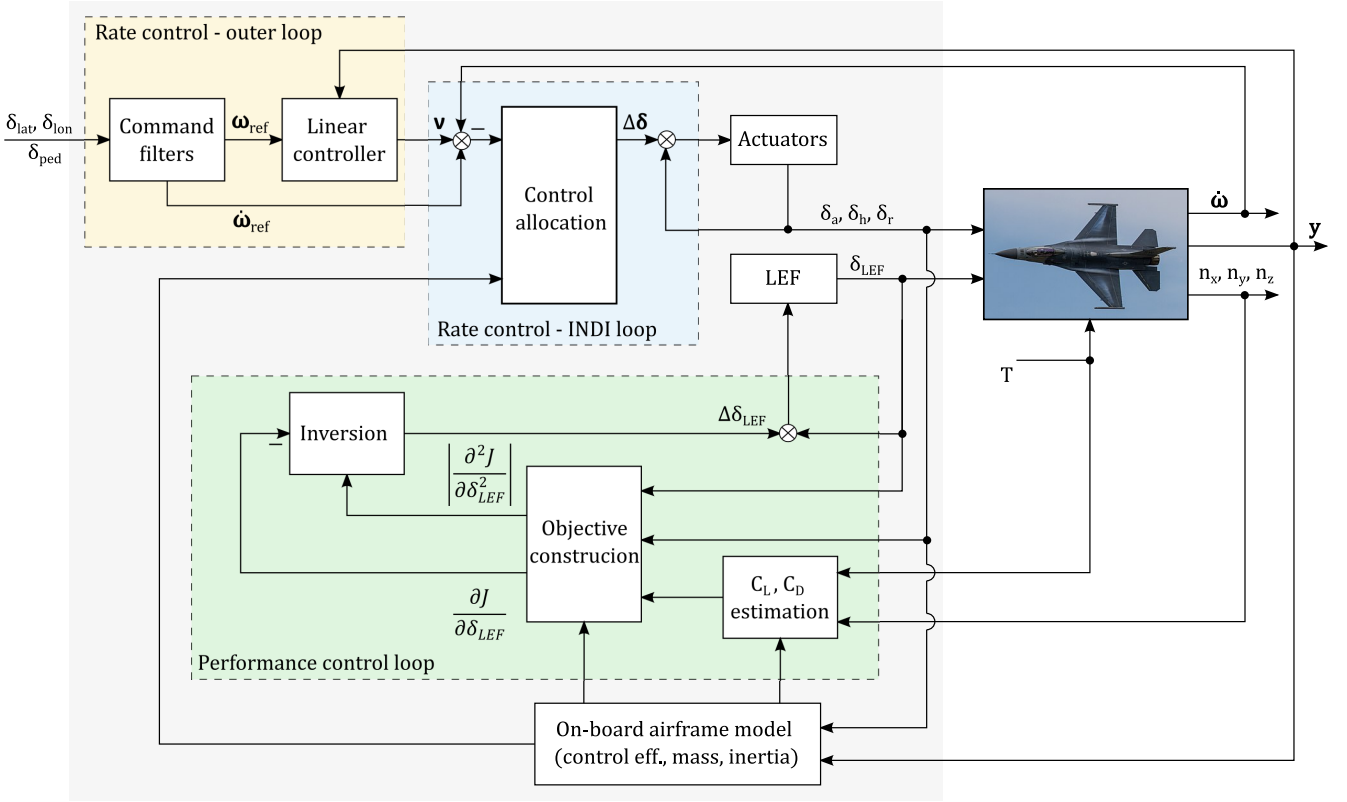
Fig. 1   Control system overview

$\eta_{\delta_h}(\delta_h) = 1$ for the deflection ranges considered in this study. It should be noted that the aerodynamic model equations are affine only in terms of the leading edge flap position.

3.3 Control Law Design

As indicated in Subsection 3.1, the F-16 control architecture enables isolation of functionality in different parts of the control system. Accordingly, the control law design process is split in two steps. First, an INDI-based angular rate control law is developed to address handling quality requirements based on horizontal tail (δ_h), flaperon (δ_a), and rudder (δ_r) commands. Secondly, an incremental optimal control law is constructed that automatically instructs the leading edge flap (δ_{LEF}) to optimize the aerodynamic performance of the airframe. Figure 1 illustrates an overview of the complete control system.

3.3.1 Angular rate control

The derivation starts with the basic formulation of rotational kinematics in the body frame:

$$\dot{\omega} = J^{-1}\left(M(x,u) - \omega \times J\omega\right) \tag{17}$$

where in this context J represents the inertia matrix and $\omega \triangleq \begin{bmatrix} p & q & r \end{bmatrix}^T$. Since the input vector appears directly in the equation, the Taylor expansion can be performed to arrive at the input-affine incremental formulation. Defining $\delta \triangleq \begin{bmatrix} \delta_a & \delta_h & \delta_r \end{bmatrix}^T$ as the vector of available control surface inputs,

$$\dot{\omega} = \dot{\omega}_0 + \frac{\partial}{\partial x}\left[J^{-1}\left(M(x,u) - \omega \times J\omega\right)\right]\Delta x + \frac{\partial}{\partial \delta}\left[J^{-1}\left(M(x,u) - \omega \times J\omega\right)\right]\Delta \delta$$
$$+ \frac{\partial}{\partial \delta_{LEF}}\left[J^{-1}\left(M(x,u) - \omega \times J\omega\right)\right]\Delta \delta_{LEF} + R_1 \tag{18}$$

Leveraging the time-scale separation assumption and omitting[2] the leading-edge flap contribution yields the INDI control law,

$$\delta = \delta_0 + \hat{M}_\delta^{-1}(x_0, u_0) J [\nu - \dot{\omega}_0] \tag{19}$$

where $M_\delta(x,u) \triangleq \frac{\partial M(x,u)}{\partial \delta}$. The pseudo-control vector is generated by an outer loop two degree-of-freedom linear proportional integrator (PI) control law, as defined by

$$\nu = \dot{\omega}_{ref} + \mathbf{K}_P \left(\omega_{ref} - \omega \right) + \mathbf{K}_I \int \left(\omega_{ref} - \omega \right) \mathrm{dt} \tag{20}$$

The nature of this design brings the advantage that the nominal airframe response to pilot input can be designed largely independently from the disturbance rejection dynamics. The desired control inceptor to aircraft rate response is formulated explicitly using the following command filters:

$$\frac{q_{ref}(s)}{\delta_{lon}(s)} = \frac{K_q(T_{\theta_2} s + 1)}{s^2 + 2\zeta_{sp}\omega_{sp}s + \omega_{sp}^2} \tag{21}$$

$$\frac{p_{ref}(s)}{\delta_{lat}(s)} = \frac{K_p}{s + \tau_p}, \qquad \frac{r_{ref}(s)}{\delta_{ped}(s)} = \frac{K_r}{s + \tau_r} \tag{22}$$

where δ_{lat}, δ_{lon}, δ_{ped} represent lateral and longitudinal stick and pedal inputs, respectively. The pitch and roll command filters are consistent with the desired LOES response as described by MIL-STD-1797A [1]. For the yaw axis, yaw rate is generally not commanded directly as suggested here but follows from another control loop that regulates the sideslip angle β to achieve desirable handling qualities. However, this is outside the scope of the present study.

3.3.2 Airframe performance control

Central to the performance control law is the specification of an adequate objective function J, which needs to reflect the primary design goals specified in Table 1. In this view, the following performance index is proposed:

$$J(x,u) = \frac{1}{2} \left(\left[\frac{C_L}{C_D} \right]_{max} \frac{C_D}{C_L} \right)^2 + \frac{1}{2} \frac{k}{\delta_{LEF,max}^2} \left(\delta_{LEF} - \frac{\Delta C_{m_{\delta_h}}(\alpha, \beta, \bar{\delta}_h)}{C_{m_{\delta_{LEF}}}} \right)^2 \tag{23}$$

where

$$\Delta C_{m_{\delta_h}}(\alpha, \beta, \delta_h) \triangleq C_m(\alpha, \beta, \delta_h) - C_m(\alpha, \beta, \delta_h = 0°) \tag{24}$$

and $\bar{\delta}_h$ represents the low-frequency trim component of the horizontal tail activity, which is obtained by passing the position measurement through a first-order low-pass filter,

$$\bar{\delta}_h(s) = \frac{\tau_{trim}}{s + \tau_{trim}}(s) \delta_h(s) \tag{25}$$

---

[2]For a complete dynamic inversion control law design, all control effectors should be incorporated or allocated in an integrated fashion to account for coupling effects. However, explicitly incorporating the incremental contribution of the LEF does not add significantly to the performance of the rate control law in the presented scenario.

The rationale behind the suggested objective function is threefold. First, maximization of C_L/C_D implies that its inverse shall be selected as the optimal control target, which forms the first part of the definition. Second, the nature of the design objectives listed in Subsection 3.1 implies that a balance needs to be found, which calls for design decisions. Specifically, the desire for minimizing control activity, combined with the need to mitigate undesirable transients to maintain satisfactory handling qualities, shall be traded against maximizing aerodynamic efficiency. This leads to the inclusion of the second term in J, which represents the normalized difference in low-frequency moment generated by the leading edge flap and the horizontal tail. Keeping this term small ensures that the aircraft trim configuration varies slowly with flight condition. Finally, all terms are normalized such that J and the objective weighting parameter k become dimensionless. The optimal control design process proceeds by finding the first and second-order derivatives of J with respect to δ_{LEF}. Consequently,

$$
\begin{aligned}
\frac{\partial J(x,u)}{\partial \delta_{LEF}} &= \left[\frac{C_L}{C_D}\right]_{max}^2 \frac{C_D}{C_L} \frac{\partial(C_D/C_L)}{\partial \delta_{LEF}} + \frac{k}{\delta_{LEF,max}^2}\left(1 - \frac{C_{m_{\delta_h}}}{C_{m_{\delta_{LEF}}}}\frac{\partial \bar{\delta}_h}{\partial \delta_{LEF}}\right)\left(\delta_{LEF} - \frac{\Delta C_{m_{\delta_h}}(\alpha,\beta,\bar{\delta}_h)}{C_{m_{\delta_{LEF}}}}\right) \\
&= \left[\frac{C_L}{C_D}\right]_{max}^2 \frac{C_D}{C_L} \frac{\partial(C_D/C_L)}{\partial \delta_{LEF}} + \frac{2k}{\delta_{LEF,max}^2}\left(\delta_{LEF} - \frac{\Delta C_{m_{\delta_h}}(\alpha,\beta,\bar{\delta}_h)}{C_{m_{\delta_{LEF}}}}\right)
\end{aligned}
\tag{26}
$$

The second equality holds thanks to the angular rate control law, which ensures robust compensation of low-frequency leading edge flap contributions in the pitching moment as reflected by

$$
\frac{\partial \bar{\delta}_h}{\partial \delta_{LEF}} = -\frac{C_{m_{\delta_{LEF}}}}{C_{m_{\delta_h}}}
\tag{27}
$$

Proceeding with the second-order derivative,

$$
\begin{aligned}
\frac{\partial^2 J(x,u)}{\partial \delta_{LEF}^2} &= \left[\frac{C_L}{C_D}\right]_{max}^2 \left(\left(\frac{\partial(C_D/C_L)}{\partial \delta_{LEF}}\right)^2 + \frac{C_D}{C_L}\frac{\partial^2(C_D/C_L)}{\partial \delta_{LEF}^2}\right) + \frac{4k}{\delta_{LEF,max}^2} \\
&= \left[\frac{C_L}{C_D}\right]_{max}^2 \frac{\partial(C_D/C_L)}{\partial \delta_{LEF}}\left(\frac{\partial(C_D/C_L)}{\partial \delta_{LEF}} - 2\frac{C_{L_{\delta_{LEF}}}C_D}{C_L^2}\right) + \frac{4k}{\delta_{LEF,max}^2}
\end{aligned}
\tag{28}
$$

where again the equality from Equation 27 has been used. Moreover, the fact that the derivative of C_D/C_L with respect to the LEF position can be found explicitly has been exploited:

$$
\frac{\partial(C_D/C_L)}{\partial \delta_{LEF}} = \frac{C_{D_{\delta_{LEF}}}C_L - C_{L_{\delta_{LEF}}}C_D}{C_L^2}
\tag{29}
$$

Finally, the lift and drag coefficients can be estimated from IMU (n_x, n_y, n_z) and thrust (T) measurements based on basic flight dynamics principles, as follows from the relations

$$
\hat{C}_X = \frac{mg}{\bar{q}S}n_x^{CG} - \frac{1}{\bar{q}S}T, \quad \hat{C}_Y = \frac{mg}{\bar{q}S}n_y^{CG}, \quad \hat{C}_Z = -\frac{mg}{\bar{q}S}n_z^{CG}
\tag{30}
$$

and the transformation from the body-fixed to the aerodynamic reference frame, as given by

8

$$\hat{C}_D = -\cos(\alpha)\cos(\beta)\hat{C}_X - \sin(\beta)\hat{C}_Y - \sin(\alpha)\cos(\beta)\hat{C}_Z$$
$$\hat{C}_L = \sin(\alpha)\hat{C}_X - \cos(\alpha)\hat{C}_Z \tag{31}$$

Consequently, this leads to the final incremental optimal control law

$$\delta_{LEF} = \delta_{LEF_0} - \left[\left\| \frac{\widehat{\partial^2 J(x,u)}}{\partial \delta_{LEF}^2} \right\| \right]_0^{-1} \left[\frac{\widehat{\partial J(x,u)}}{\partial \delta_{LEF}} \right]_0 \tag{32}$$

This result depends on on-board model representations of the control effectiveness contributions $C_{L_{\delta_{LEF}}}(\alpha,\beta)$, $C_{D_{\delta_{LEF}}}(\alpha,\beta)$, $C_{m_{\delta_{LEF}}}(\alpha,\beta)$, $\Delta C_{m_{\delta_h}}(\alpha,\beta,\delta_h)$ only, combined with sensor measurements of the linear accelerations, aerodynamic angles, control surface positions, and engine thrust. It should be noted that the implemented control law features a small protection bandwidth around $C_L = 0$ as a safeguard against singularities. As a final remark, the incremental contribution of δ_h to the Taylor expansion of Equation 26 has been omitted in the obtained control law. The result is that dynamic coupling effects with the horizontal tail are not directly compensated for; however, this comes at the benefit of a reduction in design complexity.

4 Simulation Results

In this Section, the control system design is adopted in a nonlinear simulation study. A single pull-up/push-over simulation scenario will be considered, corresponding to a straight-and-level trim flight condition of Mach 0.4 at 10,000 feet altitude, with the center of gravity located at 38% relative to the mean aerodynamic chord (MAC). This corresponds to a trim angle-of-attack of 4.4°. To investigate the effect of changing flight conditions, the throttle is moved back to idle at the start of the simulation, causing the aircraft to decelerate. Nominal performance results are presented first in Subsection 4.1, which is followed by an examination of robustness properties in Subsection 4.2.

4.1 Nominal Performance

In order to make an informed assessment of the aerodynamic performance delivered by the incremental control system, a benchmark design that adopts the default leading edge flap schedule is used for comparison. The default schedule is formulated as [28],

$$\delta_{LEF}(s) = 1.38 \frac{2s + 7.25}{s + 7.25}\alpha - 9.05\frac{\bar{q}}{p_s} + 1.45 \tag{33}$$

where $\bar{q}/p_s$ represents the ratio of free-stream dynamic pressure over static pressure. Figures 2 and 3 visualize the simulation time histories with the objective weighting parameter k set to 0 and 1, respectively. Both designs succeed in generating the desired pitch rate response dictated by the command filter from Equation 21 and improving the aerodynamic efficiency over the uncommanded (trim) LEF design, which implies that design objective *AP.1* is considered appropriately in the design. Efficiency gains compared to the default scheduled design are also visible. However, the $k = 0$ variant fails to perform satisfactory on other criteria, as the limited objective function definition does not lead to a balanced design. In particular, high-order transients are present in the vertical load factor response during the pitch-up maneuver, leading to deteriorated handling qualities and thereby not meeting requirement *HQ.1*. Similarly, it appears that a critical point is transcended as the angle-of-attack moves beyond $5-6°$, which leads to a full LEF command in the absence of stick input. Evidently, this implies that the design scores poorly in terms of criteria *HQ.2* and *CE.1* as well.
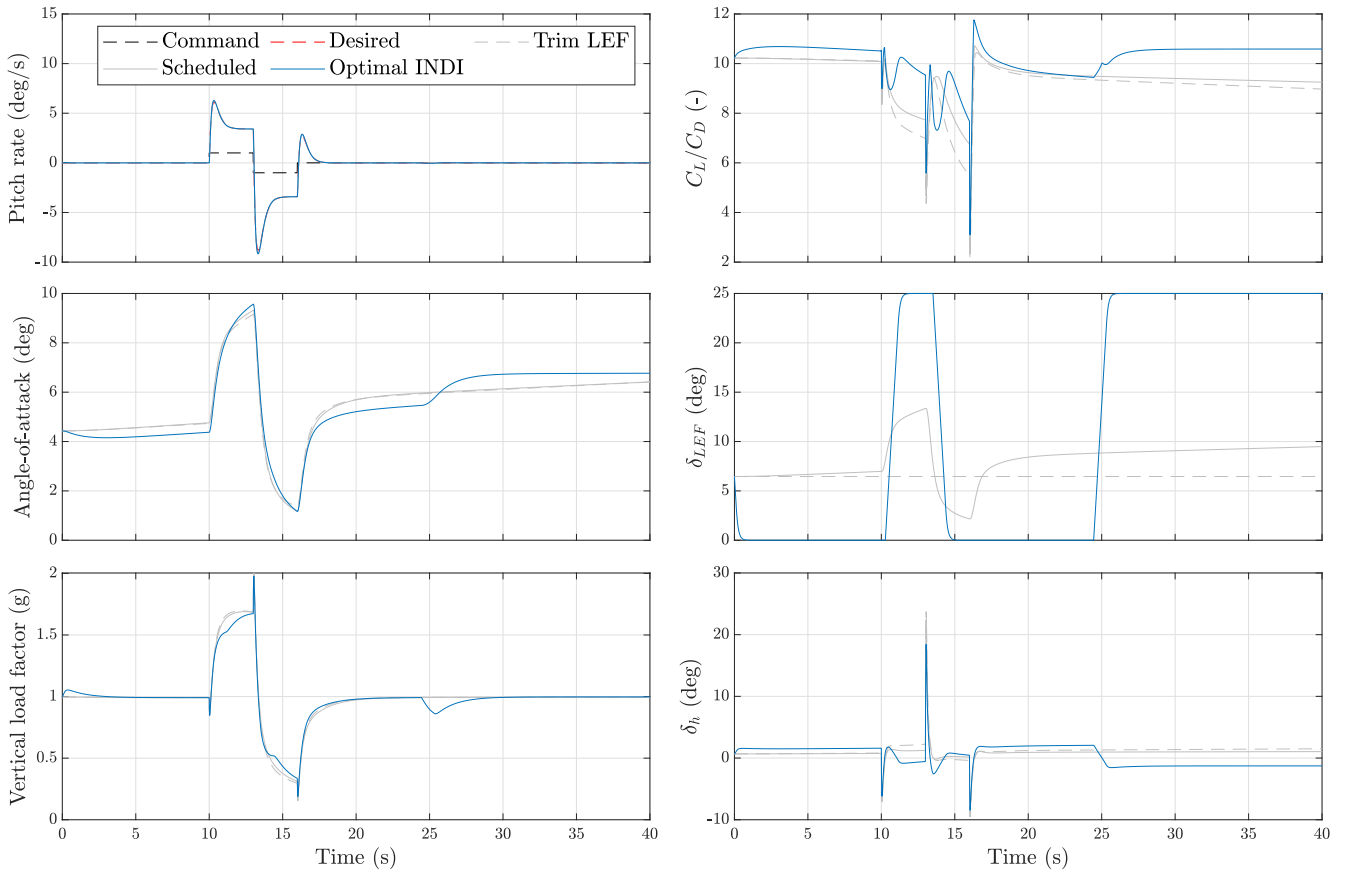
Fig. 2 Simulation scenario time histories, objective weighting parameter $k = 0$
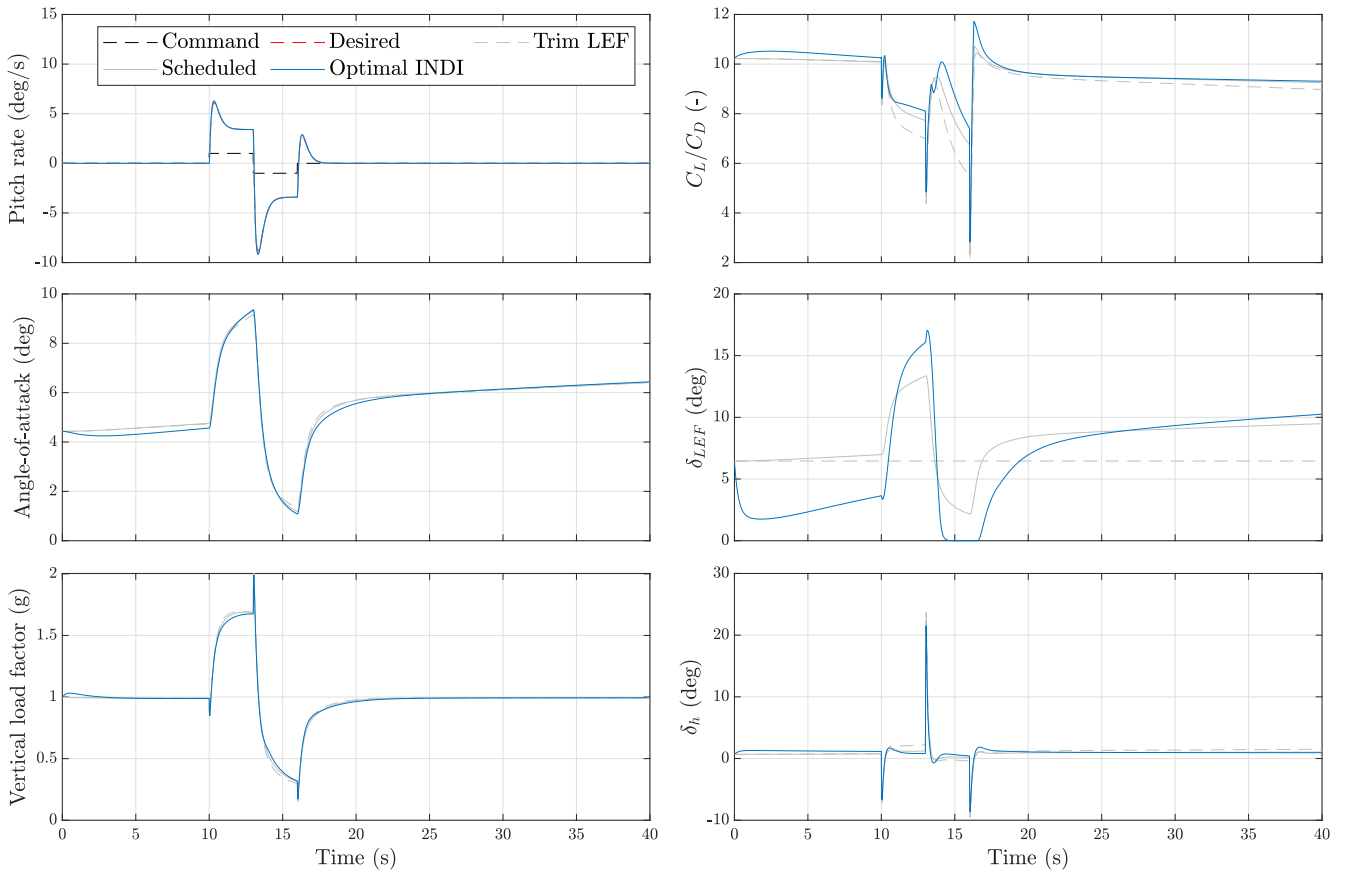

Fig. 3 Simulation scenario time histories, objective weighting parameter $k = 1$

By contrast, setting $k = 1$ leads to a better balanced design, with both pitch rate and load factor response being very close to the benchmark and improved aerodynamic efficiency levels at the absence of sudden transients and high control activity. It should be noted that the observed non-minimum phase (NMP) behavior in the LEF deflection time history is due to the direct contribution of the horizontal tail to the lift and drag coefficients, which is not compensated for in this design.

4.2 Robustness Properties

The robustness properties of the proposed airframe performance control law are examined in the context of uncertainty in the model elements that constitute the control law described by Equation 32.
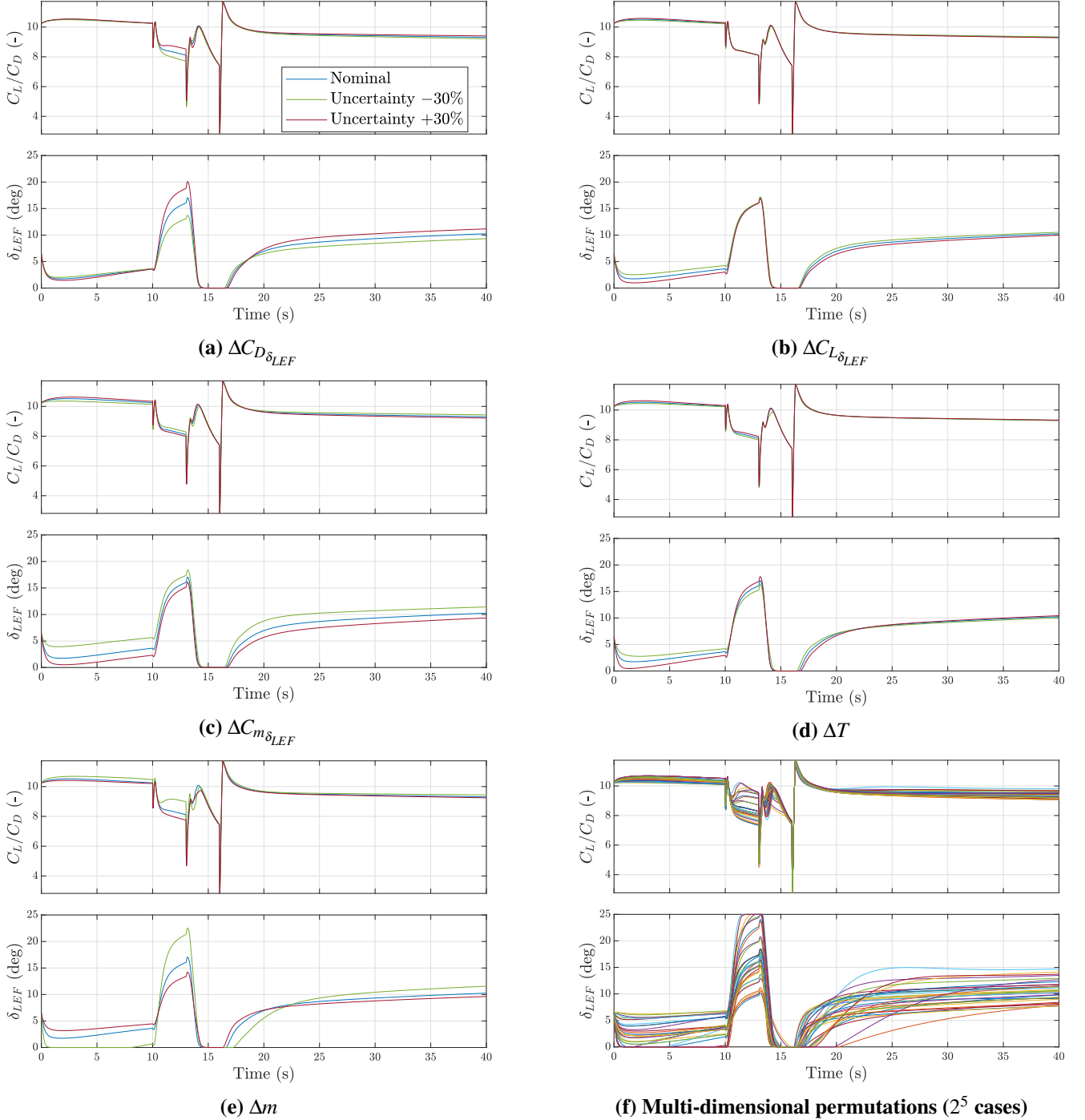

(a) $\Delta C_{D_{\delta_{LEF}}}$

(b) $\Delta C_{L_{\delta_{LEF}}}$

(c) $\Delta C_{m_{\delta_{LEF}}}$

(d) ΔT

(e) Δm

(f) Multi-dimensional permutations (2^5 cases)

Fig. 4   Robustness time histories for on-board model offsets of $\pm 30\%$, as obtained for single-dimensional and multi-dimensional permutations

Figure 4 gives an overview of the time histories obtained for the LEF position and aerodynamic efficiency levels when subjected to on-board representation offsets of $\pm 30\%$. It is apparent from these results that the control law is most sensitive to uncertainty in $C_{D_{\delta_{LEF}}}$ and aircraft mass m. These parameters may not be easy to obtain; the former can be particularly problematic to predict accurately [31]. Altogether, based on these results it can be concluded that the observed robustness properties of the proposed incremental optimal control law are less beneficial compared to what is commonly observed for traditional INDI control laws [26].

5 Conclusion

The proposed incremental optimal control framework has been demonstrated to be a viable strategy for optimizing vehicle performance objectives using limited model information. Consequently, it represents a potential design tool to improve in-operation efficiency levels despite the challenges posed by aerodynamics that are difficult to identify and model. Still, there are many open research directions that require future consideration. Several will be mentioned here.

First, the robustness characteristics demonstrated in the nonlinear simulation scenario cannot be considered as highly beneficial, especially when considering the difficulties that may arise in identifying the control effectiveness associated with the drag coefficient and estimating aircraft mass in-flight. Therefore, new directions shall be found to address this challenge. This also extends to an examination of stability margins, which will be affected by the LEF feedback logic. Second, the consequences of applying the time-scale separation assumption in the derivation of the incremental optimal control framework need to be further investigated. This is a relevant research direction, since the assumption forms a key aspect of the presented theory. Third, the proposed framework shall be developed further to enable full integration with INDI-based feedback laws, enabling true multi-functional design architectures. Such a strategy does not rely on isolation of individual control effectors as in this work, but would allocate effector suites in an optimal fashion instead. Finally, to advance the overall maturity of the concept, flight test demonstrations shall be performed on a suitable platform.

References

[1] Anonymous. Flying Qualities of Piloted Aircraft. Technical Report MIL-HDBK-1797A, U.S. Department of Defense (DoD), 1997.

[2] Anonymous. Flight Control Systems - Design, Installation, and Test of Piloted Aircraft, General Specification for. Technical Report MIL-DTL-9490E, U.S. Department of Defense (DoD), 2008.

[3] M. Wagner and G. Norris. *Boeing 787 Dreamliner*. Zenith Press, 2009.

[4] D. Reckzeh. Multifunctional Wing Moveables: Design of the A350XWB and the Way to Future Concepts. In *Proceedings of the 29th Congress of the International Council of the Aeronautical Sciences (ICAS)*, St. Petersburg, Russia, 2014.

[5] K. Bordignon and J. Bessolo. Control Allocation for the X-35B. In *Proceedings of the 2002 Biennial International Powered Lift Conference and Exhibit*, Williamsburg, VA, USA, 2002. AIAA 2002-6020. DOI: 10.2514/6.2002-6020.

[6] J. J. Harris. F-35 Flight Control Law Design, Development and Verification. In *Proceedings of the 2018 Aviation Technology, Integration, and Operations Conference*, Atlanta, GA, USA, 2018. AIAA 2018-3516. DOI: 10.2514/6.2018-3516.

[7] M. A. Counts, B. Kiger, J. Hoffschwelle, A. Houtman, and G. Henderson. F-35 Air Vehicle Configuration Development. In *Proceedings of the 2018 Aviation Technology, Integration, and Operations Conference*, Atlanta, GA, USA, 2018. AIAA 2018-3367. DOI: 10.2514/6.2018-3367.

[8] S. Sieberling, Q. P. Chu, and J. A. Mulder. Robust Flight Control Using Incremental Nonlinear Dynamic Inversion and Angular Acceleration Prediction. *Journal of Guidance, Control, and Dynamics*, 33(6):1732–1742, 2010. DOI: 10.2514/1.49978.

[9] P. Simplício, M. D. Pavel, E. van Kampen, and Q. P. Chu. An acceleration measurements-based approach for helicopter nonlinear flight control using Incremental Nonlinear Dynamic Inversion. *Control Engineering Practice*, 21(8):1065 – 1077, 2013. DOI: https://doi.org/10.1016/j.conengprac.2013.03.009.

[10] E. J. J. Smeur, Q. P. Chu, and G. C. H. E. de Croon. Adaptive Incremental Nonlinear Dynamic Inversion for Attitude Control of Micro Air Vehicles. *Journal of Guidance, Control, and Dynamics*, 39(3):450–461, 2016. DOI: 10.2514/1.G001490.

[11] F. Grondman, G. Looye, R. Kuchar, Q. P. Chu, and E. Van Kampen. Design and Flight Testing of Incremental Nonlinear Dynamic Inversion-based Control Laws for a Passenger Aircraft. In *Proceedings of the 2018 AIAA Guidance, Navigation, and Control Conference*, Kissimmee, FL, USA, 2018. AIAA 2018-0385. DOI: 10.2514/6.2018-0385.

[12] T. Keijzer, G. Looye, Q. P. Chu, and E. Van Kampen. Design and Flight Testing of Incremental Backstepping based Control Laws with Angular Accelerometer Feedback. In *Proceedings of the AIAA Scitech 2019 Forum*, San Diego, CA, USA, 2019. AIAA 2019-0129. DOI: 10.2514/6.2019-0129.

[13] T. Pollack, G. Looye, and F. Van der Linden. Design and flight testing of flight control laws integrating incremental nonlinear dynamic inversion and servo current control. In *Proceedings of the AIAA Scitech 2019 Forum*, San Diego, CA, USA, 2019. AIAA 2019-0130. DOI: 10.2514/6.2019-0130.

[14] E. J. J. Smeur, M. Bronz, and G. C. H. E. de Croon. Incremental Control and Guidance of Hybrid Aircraft Applied to a Tailsitter Unmanned Air Vehicle. *Journal of Guidance, Control, and Dynamics*, 43(2):274–287, 2020. DOI: 10.2514/1.G004520.

[15] M. D. Pavel, P. Shanthakumaran, Q. P. Chu, O. Stroosma, M. Wolfe, and H. Cazemier. Incremental Nonlinear Dynamic Inversion for the Apache AH-64 Helicopter Control. *Journal of the American Helicopter Society*, 65(2):1–16, 2020. DOI: doi:10.4050/JAHS.65.022006.

[16] P. A. Scholten, M. M. van Paassen, Q. P. Chu, and M. Mulder. Variable Stability In-Flight Simulation System Based on Existing Autopilot Hardware. *Journal of Guidance, Control, and Dynamics*, 43(12):2275–2288, 2020. DOI: 10.2514/1.G005066.

[17] X. Wang, E. Van Kampen, Q. P. Chu, and R. De Breuker. Flexible Aircraft Gust Load Alleviation with Incremental Nonlinear Dynamic Inversion. *Journal of Guidance, Control, and Dynamics*, 42(7):1519–1536, 2019. DOI: 10.2514/1.G003980.

[18] X. Wang, T. Mkhoyan, and R. De Breuker. Nonlinear Incremental Control for Flexible Aircraft Trajectory Tracking and Load Alleviation. In *Proceedings of the AIAA Scitech 2021 Forum*, Virtual event, 2021. AIAA 2021-0503. DOI: 10.2514/6.2021-0503.

[19] X. Wang, T. Mkhoyan, I. Mkhoyan, and R. De Breuker. Seamless Active Morphing Wing Simultaneous Gust and Maneuver Load Alleviation. *Journal of Guidance, Control, and Dynamics*, 44(9):1649–1662, 2021. DOI: 10.2514/1.G005870.

[20] I. Matamoros and C. C. de Visser. Incremental Nonlinear Control Allocation for a Tailless Aircraft with Innovative Control Effectors. In *Proceedings of the 2018 AIAA Guidance, Navigation, and Control Conference*, Kissimmee, FL, USA, 2018. AIAA 2018-1116. DOI: 10.2514/6.2018-1116.

[21] J. Zhang, P. Bhardwaj, S. A. Raab, S. Saboo, and F. Holzapfel. Control Allocation Framework for a Tilt-rotor Vertical Take-off and Landing Transition Aircraft Configuration. In *Proceedings of the 2018 Applied Aerodynamics Conference*, Atlanta, GA, USA, 2018. AIAA 2018-3480. DOI: 10.2514/6.2018-3480.

[22] R. Stolk and C. C. de Visser. Minimum drag control allocation for the Innovative Control Effector aircraft. In *Proceedings of the 2019 CEAS Specialist Conference on Guidance, Navigation and Control (EuroGNC)*, Milan, Italy, 2019.

[23] O. Pfeifle and W. Fichter. Energy Optimal Control Allocation for INDI Controlled Transition Aircraft. In *Proceedings of the AIAA Scitech 2021 Forum*, Virtual event, 2021. AIAA 2021-1457. DOI: 10.2514/6.2021-1457.

[24] H. K. Khalil. *Nonlinear Systems*. Pearson Education. Prentice Hall, 3rd edition, 2002.

[25] B. Bacon and A. Ostroff. Reconfigurable flight control using nonlinear dynamic inversion with a special accelerometer implementation. In *Proceedings of the AIAA Guidance, Navigation, and Control Conference and Exhibit*, Denver, CO, USA, 2000. AIAA 2000-4565. DOI: 10.2514/6.2000-4565.

[26] X. Wang, E. van Kampen, Q. P. Chu, and P. Lu. Stability Analysis for Incremental Nonlinear Dynamic Inversion Control. *Journal of Guidance, Control, and Dynamics*, 42(5):1116–1129, 2019. DOI: 10.2514/1.G003791.

[27] R. L. Burden and J. D. Faires. *Numerical Analysis*. Brooks/Cole, Cengage Learning, 9th edition, 2011.

[28] L. T. Nguyen, M. E. Ogburn, W. P. Gilbert, K. S. Kibler, P. W. Brown, and P. L. Deal. Simulator Study of Stall/Post-Stall Characteristics of a Fighter Airplane With Relaxed Longitudinal Static Stability. Technical report, National Aeronautics and Space Administration, Langley Research Center, Hampton, Virginia, 1979.

[29] R. Russel. Non-linear F-16 Simulation using Simulink and Matlab. Technical report, University of Minnesota, 2003.

[30] C. Droste and J. Walker. *The General Dynamics Case Study on the F-16 Fly-By-Wire Flight Control System*. American Institute of Aeronautics and Astronautics, Inc., 2010. DOI: 10.2514/4.867873.

[31] T. S. Chyczewski, M. Dubiel, D. R. McDaniel, M. Foster, M. A. Niestroy, S. M. Klausmeyer, W. A. Silva, D. D. Vicroy, C. Hummer, W. Thomas, and B. E. Green. A Position on Current Stability and Control Prediction Capabilities and a Path Forward. In *Proceedings of the AIAA Aviation 2020 Forum*, Virtual event, 2020. AIAA 2020-2678. DOI: 10.2514/6.2020-2678.